



Electronic and optical properties of the LiCdX (X = N, P, As and Sb) filled-tetrahedral compounds with the Tran–Blaha modified Becke–Johnson density functional

A. Bouhemadou^{a,*}, S. Bin-Omran^{b,c}, D. Allali^a, S.M. Al-Otaibi^b, R. Khenata^d,
Y. Al-Douri^e, M. Chegaar^f, A.H. Reshak^{g,h}

^a Laboratory for Developing New Materials and their Characterization, University of Setif 1, Setif 19000, Algeria

^b Department of Physics and Astronomy, College of Science, King Saud University, P.O. Box 2455, Riyadh 11451, Saudi Arabia

^c Department of Physics, Faculty of Science & Humanitarian Studies, Salman Bin Abdalaziz University, Alkharj 11942, Saudi Arabia

^d Laboratoire de Physique Quantique et de Modélisation Mathématique (LPQ3M), Département de Technologie, Université de Mascara, Mascara 29000, Algeria

^e Institute of Nano Electronic Engineering, Universiti Malaysia Perlis, Kangar, Perlis 01000, Malaysia

^f Department of Physics, Faculty of Science, University of Setif 1, Setif 19000, Algeria

^g New Technologies-Research Center, University of West Bohemia, Univerzitni 8, Pilson 306 14, Czech Republic

^h Center of Excellence Geopolymer and Green Technology, School of Material Engineering, University Malaysia Perlis, Kangar, Perlis 01007, Malaysia

ARTICLE INFO

Article history:

Received 5 April 2014

Received in revised form 26 August 2014

Accepted 3 January 2015

Available online 5 January 2015

Keywords:

A. Semiconductors
D. Electronic structure
D. Optical properties

ABSTRACT

The structural, electronic and optical properties of the LiCdN, LiCdP, LiCdAs and LiCdSb filled-tetrahedral compounds have been explored from first-principles. The calculated structural parameters are consistent with the available experimental results. Since DFT with the common LDA and GGA underestimates the band gap, we use a new developed functional able to accurately describe the electronic structure of semiconductors, namely the Tran–Blaha-modified Becke–Johnson potential. The four investigated compounds demonstrate semiconducting behavior with direct band gap ranging from about 0.32 to 1.65 eV. The charge-carrier effective masses are evaluated at the topmost valence band and at the bottommost conduction band. The evolution of the value and nature of the energy band gap under pressure effect is also investigated. The frequency-dependent complex dielectric function and some macroscopic optical constants are estimated. The microscopic origins of the structures in the optical spectra are determined in terms of the calculated energy band structures.

© 2015 Elsevier Ltd. All rights reserved.

1. Introduction

The development and optimization of optoelectronic devices crucially depend on the availability of suitable semiconductor materials. The ternary and higher multinary semiconductor compounds provide a wide range of electronic and optical properties to choose for the respective technological applications. A particular interesting class of ternary materials are the eight valence electrons I–II–V type, such as the Nowotny–Juza A^IB^{II}C^V compounds [1,2] (where the Roman numerals indicate the appropriate column of the periodic table, i.e., A^I = Li, Na, Cu, Ag; B^{II} = Mg, Zn, Cd and C^V = N, P, As, Sb and Bi). The Nowotny–Juza A^IB^{II}C^V compounds are also called “filled zinc-blende structure” or “filled-tetrahedral compounds” (FTC). The filled-tetrahedral

compounds A^IB^{II}C^V (e.g., LiCdP) constitute an interesting class of generally direct gap semiconductors closely related to the more familiar III–V compounds (e.g., InP is the binary analogous to LiCdP) [3–7]. A number of these materials were synthesized and structurally characterized by Nowotny [1] and Juza [2] a long time ago. Interest in this family compounds has been renewed since the prediction of Wood et al. [3], and Carlson et al. [4] that the filled-tetrahedral compounds LiZnP and LiZnN exhibit semiconducting character with a direct energy band gap, and hence they are very prominent materials for photovoltaic and some other technological applications. This prediction has stimulated numerous experimental and theoretical works; consequently several compounds of this class have been synthesized and characterized [5–38].

Most of the filled-tetrahedral compounds A^IB^{II}C^V (e.g., LiCdP) usually crystallize in a cubic structure which can be obtained from the zinc-blende D^{III}C^V (e.g., InP) by transmuted the D^{III} (e.g., In atom) to the isovalent A^I+B^{II} (Li+Cd) atom pair. The familiar

* Corresponding author. Tel.: +213 553163456; fax: +213 36620136.

E-mail address: a_bouhemadou@yahoo.fr (A. Bouhemadou).

zinc-blende structure (space group $F\bar{4}3m$) can be characterized by four lattice sites in the conventional cell, namely $\tau_1=(0,0,0)$, $\tau_2=(0.25,0.25,0.25)$, $\tau_3=(0.5,0.5,0.5)$, and $\tau_4=(0.75,0.75,0.75)$. The zinc-blende structure of a $D^{III}C^V$ compound (e.g., InP) has the D^{III} atom (e.g., In) at $\tau_1=(0,0,0)$, the C^V atom at $\tau_2=(0.25,0.25,0.25)$, and two empty interstitial sites at $\tau_3=(0.5,0.5,0.5)$ (next to the anion) and $\tau_4=(0.75,0.75,0.75)$ (next to the cation). The crystal structure of the cubic Nowotny–Juza $A^I B^{II} C^V$ can be described as follows: the B^{II} and C^V atoms form a regular zinc-blende crystal, and the A^I atom can occupy either the $\tau_3=(0.5,0.5,0.5)$ site (next to the column V anion), and forms the α -phase or the $\tau_4=(0.75,0.75,0.75)$ site (next to the column II cation) to form the β -phase. The γ -phase can be obtained when the two sites are occupied. The space group of the cubic $A^I B^{II} C^V$ is $F\bar{4}3m$ as well as a zinc-blende structure. In the most stable cubic arrangement of the atoms of the $A^I B^{II} C^V$ compound, the alkali atom (e.g., A^I) is at the tetrahedral interstitial site nearest to the column V anion (making the later eightfold coordinated) in a conventional zinc-blende unit-cell, e.g., the α -phase, so in the present work we explore only this structure.

The $LiCdX$ ($X=N, P, As$ and Sb) compounds, belonging to the Nowotny–Juza filled tetrahedral structures, have been the subject of several experimental [6,7,39] and theoretical studies [21,23–25,34,35,38], motivated by the interest in their importance in photovoltaic and optoelectronic devices [24]. Previous theoretical studies focused on structural, elastic, vibrational, electronic and optical properties of these materials within the framework of density functional theory (DFT) with the standard local density approximation (LDA) and generalized gradient approximation (GGA) to the exchange–correlation potential, which are known to severely underestimate the band gap of the semiconductor and insulator materials [40]. The DFT with the common LDA and GGA yields satisfactory structural parameters which are in fairly good agreement with experiment but give unsatisfactory electronic properties (such as band gap and effective masses). Typically, the band gap values calculated using the DFT with the common LDA and GGA approximations are approximately 30–50% smaller than the experimental values [41,42].

Accurately calculating the electronic structure of materials is important for understanding and predicting some of their properties and technological applications. Therefore, we think it is time to perform more investigation of the electronic and optical properties of $LiCdP$ and $LiCdAs$ materials by employing highly accurate approximations to the exchange–correlation potential;

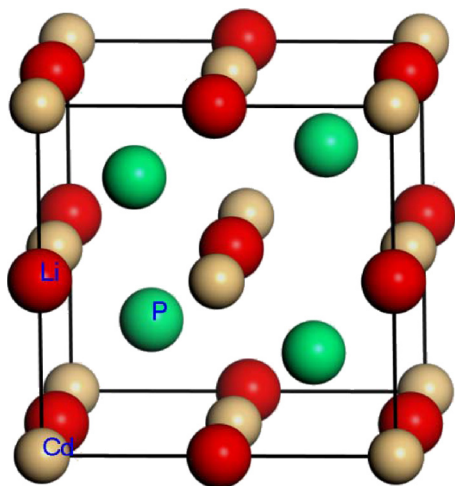


Fig. 1. The cubic crystal structure of the Nowotny–Juza filled-tetrahedral compounds $LiCdN$.

Table 1

Calculated lattice constant a_0 (in Å), bulk modulus B (in GPa), and the pressure derivative of the bulk modulus B' for the $LiCdN$, $LiCdP$, $LiCdAs$ and $LiCdSb$ compounds along with the available experimental and theoretical results in the literature.

System	Present work		Experiment	Previous calculations
	LDA	GGA		
$LiCdN$				
a_0	5.2355	5.3039		5.388 ^d , 5.22 ^g
B_0	110.32	98.36		90.911 ^d , 108.3 ^g ,
B'	4.6168	4.6671	6.087 ^a , 6.096 ^b	4.19 ^d , 3.94 ^g ,
$LiCdP$				
a_0	5.9817	6.0540		6.118 ^a , 6.137 ^d , 6.13 ^e , 6.02 ^f , 5.98 ^g , 5.9629 ⁱ ,
B_0	66.4652	60.1585		52.8 ^a , 54.965 ^d , 66.22 ^g , 67 ⁱ
B'	4.5532	4.0758	6.263 ^c	4.042 ^d , 4.44 ^g , 3.94 ⁱ
$LiCdAs$				
a_0	6.1624	6.2442		6.345 ^d , 6.016 ^f , 6.16 ^g , 6.1334 ^h ,
B_0	58.4475	53.0565		46.265 ^d , 58.62 ^g , 58.9 ^h ,
B'	4.5564	4.6485		4.042 ^d , 4.43 ^g , 3.90 ^h
$LiCdSb$				
a_0	6.5471	6.6337		
B_0	47.6940	42.9235		
B'	4.7249	4.6252		

^a [21].

^b [6].

^c [7].

^d [38].

^e [55].

^f [24].

^g [23].

^h [35].

ⁱ [34].

this constitutes the first purpose of the present work. On other side, to the best of our knowledge, the electronic and optical properties of $LiCdN$ and $LiCdSb$ compounds are not yet explored, therefore, the prediction of these properties of these compounds constitutes the second objective of this work.

At present some approximations beyond the standard LDA and GGA, such as GW, hybrid functionals (B3LYP, HSE . . .), LDA + U, LDA + DMFT . . . etc, are developed in order to accurately describe the electronic structure of semiconductors and insulators. However, some of these methods are computationally expensive or not satisfactory in all cases [43]; for example the LDA + U method can only be applied to correlated and localized electrons. Fortunately, a very elegant approach solving this dilemma has been recently suggested by Tran and Blaha [44]; the so called Tran–Blaha modified Becke–Johnson (TB–mBJ) potential approximation, and implemented in the new version of WIEN2K code [45]. The underestimation of the band gaps of semiconductors and insulators when using LDA (GGA) is due to the fact that LDA (GGA) cannot describe exactly the exchange–correlation potential. The TB–mBJ exchange potential [44] was developed from a semi-classical exchange potential proposed by Becke and Johnson [46] to reproduce the shape of the exact-exchange optimized-effective potential of atoms. The exchange–correlation potential functional TB–mBJ resulting from the combination of mBJ exchange with LDA correlation describes better the exchange–correlation potential than the LDA (GGA). The TB–mBJ can produce accurate semiconductor gaps for sp semiconductors, wide-band-gap semiconductors and transition-metal oxide semiconductors [44,47–50]. Therefore, the TB–mBJ is an alternative way to have a band gap close to the experimental value but computationally cheaper than the expensive hybrid functionals and GW methods. The TB–mBJ potential is computationally as cheap as LDA or GGA.

Therewith, one can obtain accurate band gaps. Detailed description of the TB-mBJ and its merits and limits can be found in Refs. [44–50]. Tran and Blaha [44] have demonstrated that the TB-mBJ potential yields band gaps which are in good agreement with experiment, leading to typical errors of less than 10% for some semiconductors and insulators. In the present work, we aim to calculate the electronic and optical properties of the LiCdN, LiCdP, LiCdAs, and LiCdSb materials, using the LDA [51], GGA-PBESol [52] and Engel-Vosko scheme of the GGA (GGA-EV) [53] functionals and to compare that to the obtained results using the TB-mBJ functional [44–46] in order to show the advantage of the TB-mBJ for describing electronic structure of the considered materials.

The remainder of the paper is organized as follows: In Section 2, a brief outline of the method of calculation is given. The obtained results and some discussions are presented in Section 3. Some concluding remarks are given in Section 4.

2. Computational details

Ab initio calculations were performed in the framework of density functional theory (DFT) with an all-electron method using the linearized/augmented plane wave + local orbitals (L/APW+lo) basis set as implemented in the WIEN2k code [45]. In this method, the wave functions are expanded in a linear combination of radial functions time spherical harmonics inside the non-overlapping muffin-tin spheres of radius R_{MT} surrounding each atom and in plane waves in the interstitial region between the spheres. The radii of the muffin-tin spheres were taken as large as possible without overlapping the spheres. The maximum l of the expansion of the wave function in spherical harmonics inside the muffin-tin

spheres was $l_{max} = 10$. A plane-wave cut-off of $K_{max} = 4.0$ (a.u.)⁻¹ is chosen for the expansion of the wave functions in the interstitial region. The k integrations over the Brillouin zone (BZ) are performed up to $10 \times 10 \times 10$ Monkstör-Pack mesh (MP) [54] (47 k -points in the irreducible Brillouin zone (IBZ)). The self-consistent calculations are considered converged when the total energy of the system is stable within 10^{-5} Ry. The exchange–correlation potential for the structural properties was calculated using the LDA [51] and the GGA based on Perdew et al. (GGA-PBESol) [52]. For the electronic properties, in addition to the LDA and the GGA, the GGA-EV [53] and the TB-mBJ [44–46], which better describe many semiconductors and insulators, were applied.

The linear optical properties of a material can be described by the complex dielectric function $\epsilon(\omega) = \epsilon_1(\omega) + i\epsilon_2(\omega)$. The imaginary part of the dielectric function $\epsilon_2(\omega)$ represents the absorption in the crystal, which can be calculated from the momentum matrix elements between the occupied and the unoccupied wave functions [55]:

$$\begin{aligned} \text{Im}\epsilon_{\alpha\beta}(\omega) &= \epsilon_2^{\alpha\beta}(\omega) \\ &= \frac{4\pi e^2}{m^2 \omega^2} \sum_{if} \int \langle f|p_{\alpha}|i\rangle \langle i|p_{\beta}|f\rangle W_i(1 - W_f)(E_f - E_i - \hbar\omega) d^3k. \end{aligned}$$

In this expression, $\langle f|p_{\alpha}|i\rangle$ and $\langle f|p_{\beta}|i\rangle$ are the dipole matrix elements corresponding to the α and β directions of the crystal (x, y or z), and $f(i)$ is the final (initial) state. W_n is the Fermi distribution function for the n th state, and E_n is the electron energy in the n th state. The real part of the frequency-dependent dielectric function

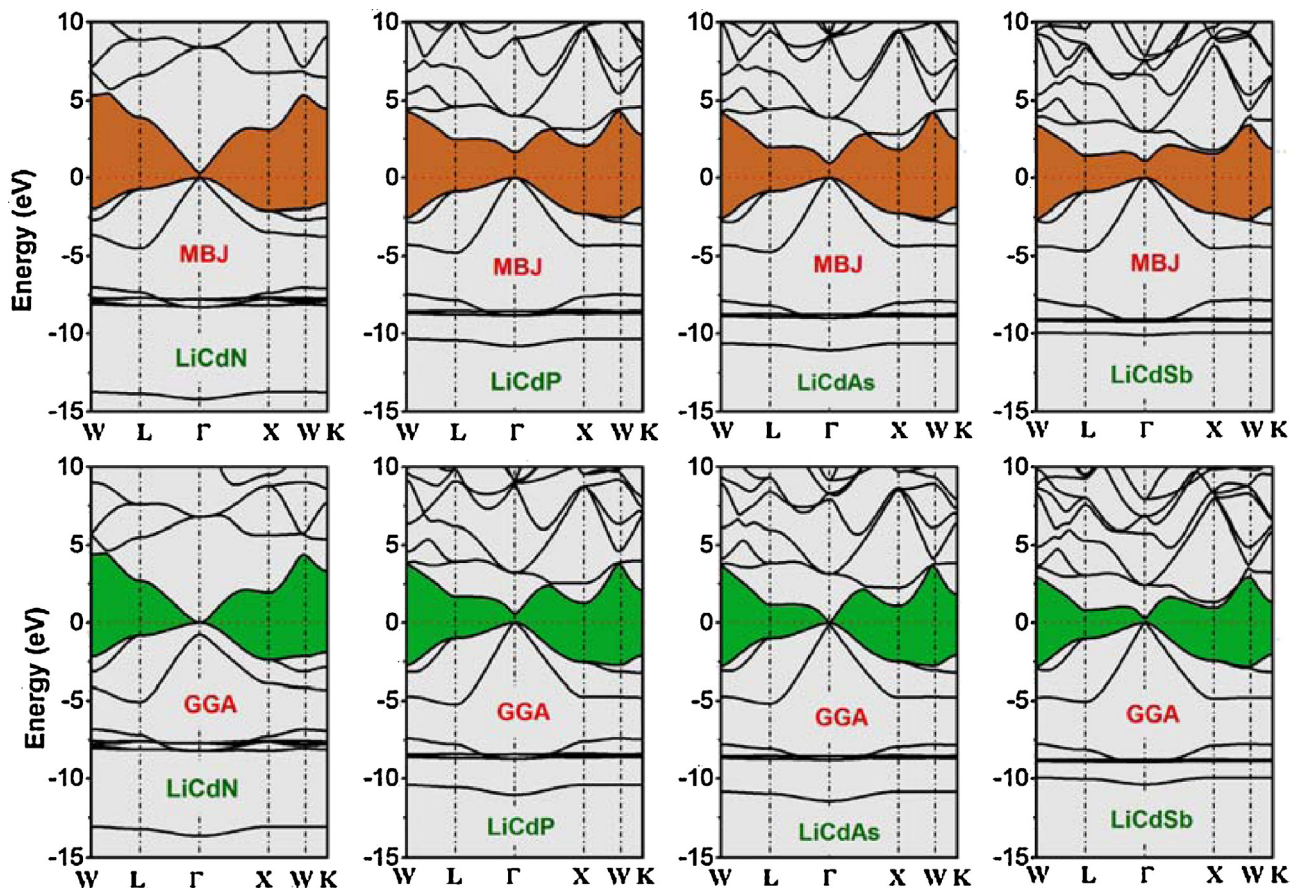


Fig. 2. The TB-mBJ and GGA-PBESol band structures of the LiCdN, LiCdP, LiCdAs and LiCdSb compounds along some high-symmetry directions of the BZ. The zero level corresponds to the Fermi level.

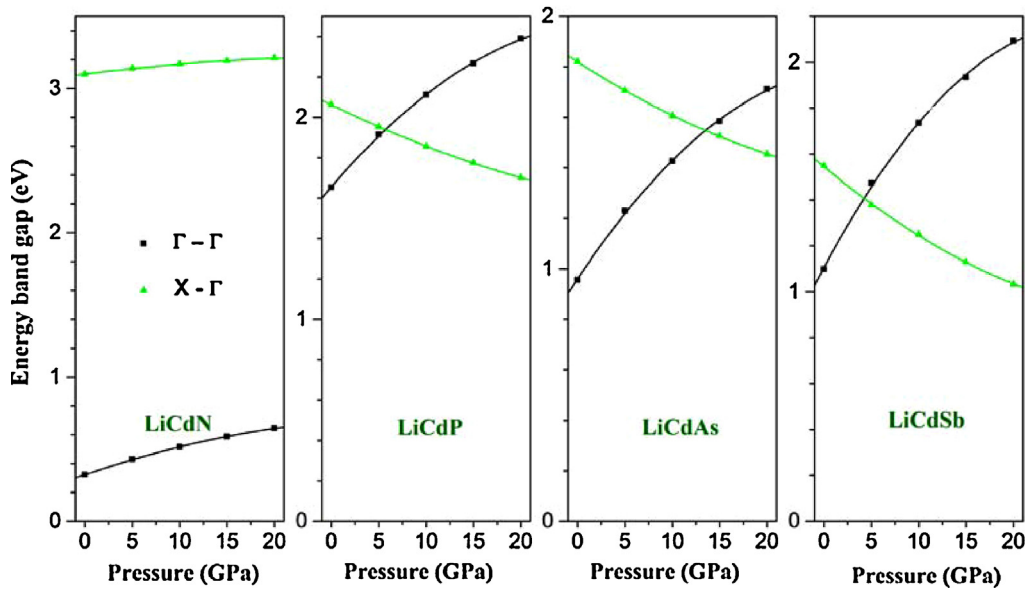


Fig. 3. Variation of the direct band gap $\Gamma-\Gamma$ and indirect band gap $\Gamma-L$ as a function of pressure for the LiCdN, LiCdP, LiCdAs and LiCdSb compounds.

expression $\epsilon_1^{\alpha\beta}(\omega)$ is computed from $\epsilon_2^{\alpha\beta}(\omega)$ using the Kramers–Kronig relations in the form:

$$\epsilon_1^{\alpha\beta}(\omega) = \delta_{\alpha\beta} + \frac{2}{\pi} P \int_0^{\infty} \frac{\omega' \epsilon_2^{\alpha\beta}(\omega')}{\omega'^2 - \omega^2} d\omega',$$

where P is the Cauchy principal value of the integral. With the knowledge of the complex dielectric tensor components all other frequency-dependent optical constants, such as the refractive index $n(\omega)$, the extinction coefficient $k(\omega)$, the reflectivity $R(\omega)$, the coefficient of absorption $\alpha(\omega)$ and the loss function $L(\omega)$, can be calculated using the well-known relations. For the cubic structure, the optical properties are isotropic, i.e., there is only one independent component (ϵ_{xx}). The optical spectra strongly depend on the BZ sampling, therefore the momentum matrix elements are explicitly evaluated at a large number of k -points in the BZ ($30 \times 30 \times 30$ k -points mesh).

Table 2

Calculated direct band gap $\Gamma-\Gamma$ and indirect band gap $\Gamma-X$ values of LiCdN, LiCdP, LiCdAs and LiCdSb with LDA, GGA-PBESol, GGA-EV and TB-mBJ functionals compared with the available literature.

	LiCdN		LiCdP		LiCdAs		LiCdSb	
	$\Gamma-\Gamma$	$\Gamma-X$	$\Gamma-\Gamma$	$\Gamma-X$	$\Gamma-\Gamma$	$\Gamma-X$	$\Gamma-\Gamma$	$\Gamma-X$
Present								
LDA	0.00	1.98	0.64	1.2	0	1.02	0.31	0.89
GGA	0.00	1.94	0.61	1.26	0	1.07	0.27	0.94
GGA-EV	0.00	2.69	1.455	2.27	0.715	2	0.94	1.56
TB-mBJ	0.32	3.1	1.65	2.06	0.96	1.82	1.1	1.55
Expt.			1.30 ^a ,					
Others	0.00 ^g		0.635 ^b , .91 ^d , 0.85 ^e ,	1.189 ^b	0.05 ^c	0.93 ^c		
			0.556 ^f	1.33 ^d	0.00 ^f			
			1.25 ^g					

^a [6].

^b [25].

^c [35].

^d [34].

^e [21].

^f [38].

^g [55].

3. Results and discussions

3.1. Structural properties

The crystal structure of LiCdN is shown in Fig. 1. The ground state properties, namely equilibrium lattice constant a , bulk modulus B and pressure derivative of the bulk modulus B' are determined by fitting the calculated total energy versus unit cell volume data to the Birch–Murnaghan equation of state [56,57]. In Table 1, we give the obtained results for the computed ground state parameters using both the LDA and GGA to the exchange–correlation potential, and make a comparison with available experimental [6,7,21] and theoretical data [21,23,34,35,38,58]. As seen in Table 1, agreement between the lattice constants (experiment and optimized) is excellent in the case of the GGA–PBESol calculations (with the largest deviation between the experimental and calculated lattice constants being 0.5% for the LiCdP). In the case of the LDA results, the maximum deviation was found to be 1.7%. It can be noted that as a result of substitutions of N by P, P by As and As by Sb, the lattice constant a increases in the following sequence: $a(\text{LiCdN}) < a(\text{LiCdP}) < a(\text{LiCdAs}) < a(\text{LiCdSb})$ (1). This trend can be easily explained by considering the atomic radii (R) of the N, P, As and Sb atoms, which increase in the same sequence: $R(\text{N}) = 0.75 \text{ \AA} < R(\text{P}) = 1.23 \text{ \AA} < R(\text{As}) = 1.33 \text{ \AA} < R(\text{Sb}) = 1.53 \text{ \AA}$. This consistency proves the reliability and the accuracy of these present *ab initio* calculation findings and gives confidence in the results of the following calculations of the electronic and optical properties for the considered materials. We did not find any experimental results for the bulk modulus B and its pressure derivative B' in the literature to support these theoretical results. Our obtained values for B and B' are reasonably consistent

Table 3

Calculated effective masses of the electron (m_e^*), the heavy hole (m_{hh}^*) and the light hole (m_{lh}^*) (in units of free electron mass m_0) for the LiCdN, LiCdP, LiCdAs and LiCdSb compounds.

	LiCdN		LiCdP		LiCdAs		LiCdSb	
	$\Gamma-L$	$\Gamma-X$	$\Gamma-L$	$\Gamma-X$	$\Gamma-L$	$\Gamma-X$	$\Gamma-L$	$\Gamma-X$
m_e^*	0.081	0.089	0.17	0.18	0.096	0.107	0.101	0.111
m_{hh}^*	2.08	0.977	1.066	0.453	0.985	0.415	0.778	0.319
m_{lh}^*	0.078	0.118	0.144	0.176	0.092	0.107	0.084	0.103

with those previously obtained using *ab initio* calculations [21,23,34,35,38]. The bulk modulus of the considered materials increase in the sequence: $B(\text{LiCdN}) > B(\text{LiCdP}) > B(\text{LiCdAs}) > B(\text{LiCdSb})$, i.e., in reverse sequence to (1); this is in agreement with the known relation between the cell volume V and the bulk modulus B : $B \sim V^{-1}$.

3.2. Electronic properties

The electronic band structures of the four considered materials are calculated with their optimized crystal structure parameters using four different functional: the LDA, the GGA–PBEsol, the GGA–EV and the TB–mBJ. We note that, because there is no exchange and correlation energy term from which the TB–mBJ potential can be deduced, a direct optimization procedure is not possible as in the usual theory [59]. The GGA–EV functional is obtained by optimizing the exchange–correlation potential V_{ex} rather than the energy E_{ex} , and it is designed to improve the band gaps rather than the local energy. Consequently, the equilibrium lattice constant calculated using this functional is considerably larger than the experimental value [60]. Therefore, the band structures using the TB–mBJ and GGA–EV functionals were calculated with the lattice parameter values that were obtained using the GGA–PBEsol functional. The overall band profiles are qualitatively similar to those previously reported [21,25,34,35,38,58], but there are quantitative differences resulting from the use of the GGA–EV and the TB–mBJ functional, and these are important. The upper valence band maximum (UVBM) and the lower conduction band minimum (LCBM) occur at Γ point; thus the four investigated materials are direct energy band gap semiconductors. In Fig. 2, we compare the band structure for LiCdN, LiCdP, LiCdAs and LiCdSb calculated with the GGA–PBEsol and with the TB–mBJ potential. As a general result, the TB–mBJ causes a rigid displacement of the conduction bands towards higher energies with respect to the top of the valence band, with small

differences in the dispersion at some regions of the Brillouin zone. The pattern of the band structures in LiCdP, LiCdAs and LiCdSb is almost similar but somewhat different from that of LiCdN, which will explain the noted differences between the optical spectra of LiCdN and the other considered compounds. After analyzing the results (Table 2), we have classified them in three groups; the first group contains the common LDA and GGA–PBEsol functionals. Both LDA and GGA–PBEsol yield a zero band gap for the LiCdN and LiCdAs compounds. The band gap value of LiCdP which is calculated within this first group is significantly less than the experimental value; there is experimental band gap value only for the LiCdP compound. The second group contains GGA–EV and predicts a band gap value for LiCdP which is comparable with the experimental result, but GGA–EV predicts a zero band gap for LiCdN. The third group contains TB–mBJ as E_{xc} functional and predicts the four considered materials as semiconductors with appreciable band gap values. There is only one experimental value for the band gap of the LiCdP compound and we have no idea about the accuracy of this measurement, therefore one needs more experimental data to make a reasonable comparison between the obtained results using TB–mBJ and the measured ones. Obviously the TB–mBJ functional significantly improves the band gap value compared to the common LDA and GGA, thus we will discuss the rest of the electronic and optical properties obtained within the TB–mBJ.

The pressure effects on the electronic and optical properties were modeled by calculating the optimized lattice parameter (a) at a set of fixed pressures ($P=0, 5, 10, 15$ and 20 GPa) then calculating these properties at these optimized geometries. The procedures to calculate the optimized lattice parameter a at a fixed pressure P are as follows: after obtaining the bulk modulus B and its pressure derivative B' according to the procedure explained in Section 3.1, the Murnaghan equation of state [56]: $V = V_0(1 + B'(P/B))^{-1/B'}$, where V_0 denotes the unit cell volume at zero pressure, is used to

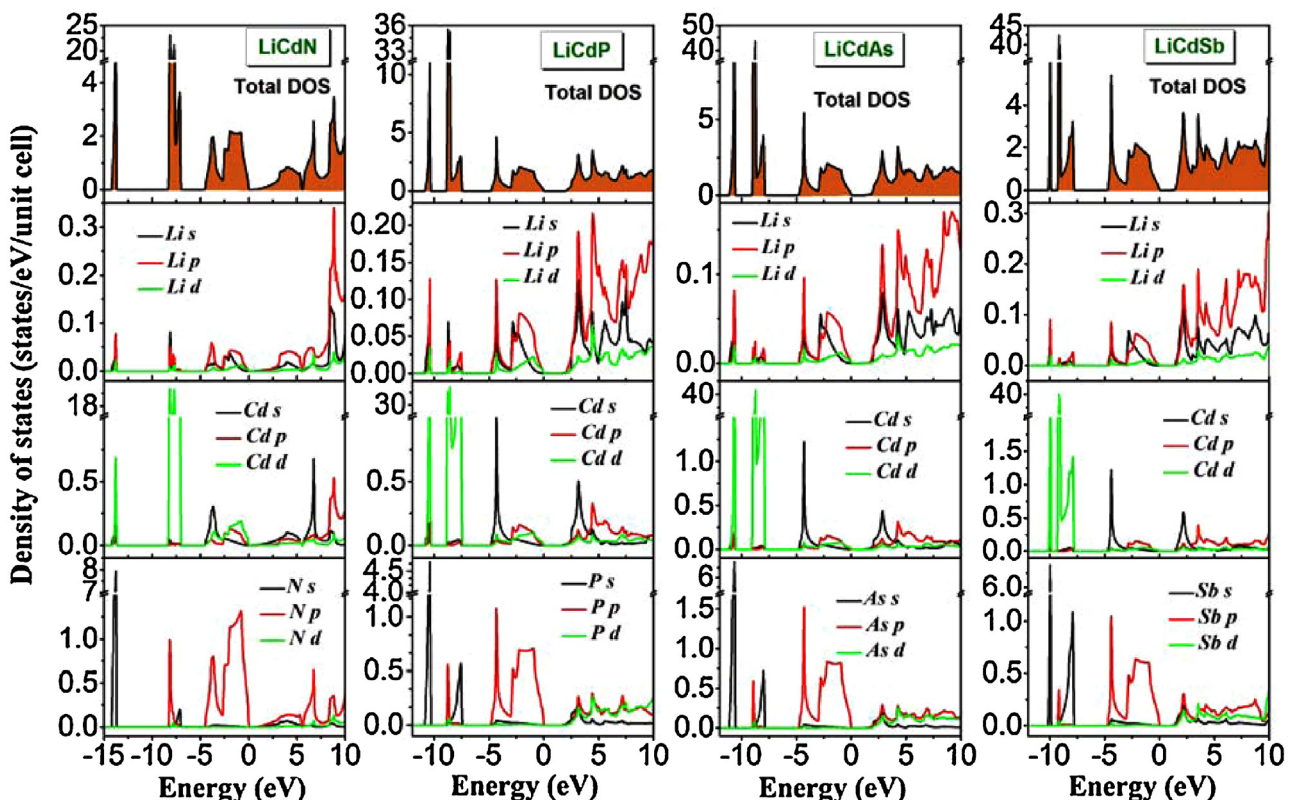


Fig. 4. The total and projected DOS diagrams of the LiCdN, LiCdP, LiCdAs and LiCdSb compounds as calculated using the TB–mBJ potential.

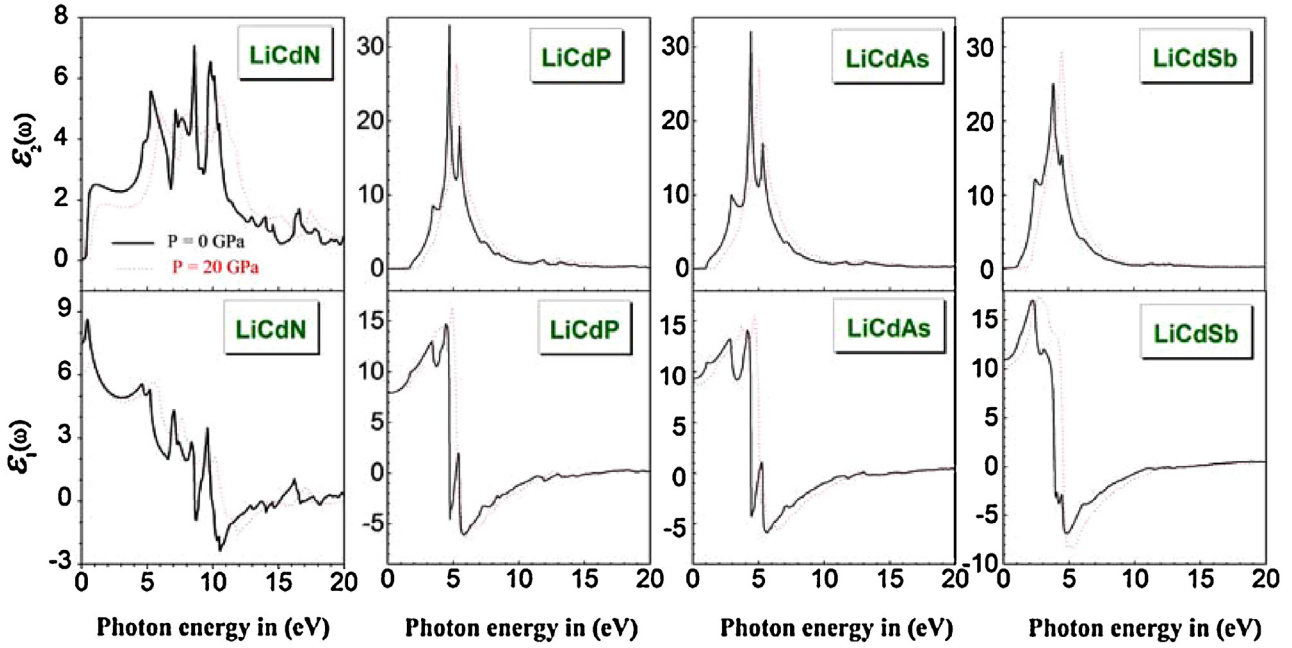


Fig. 5. The imaginary and real parts of the dielectric function (ϵ_2 and ϵ_1 , respectively) of the LiCdN, LiCdP, LiCdAs and LiCdSb compounds versus photon energy under normal and under hydrostatic pressure.

calculate the value of the unit cell volume V corresponding to the fixed pressure P then calculating the corresponding lattice parameter a . Fig. 3 shows that in the LiCdN compound, both the fundamental direct band gap Γ - Γ and the indirect band gap Γ - X increase in a non-linear manner when the pressure is enhanced. However, in the LiCdP, LiCdAs and LiCdSb compounds, when the pressure is enhanced, the fundamental direct band gap Γ - Γ increases but the indirect band gap decreases in a non-linear manner. Therefore, a crossover between the direct band gap Γ - Γ and the indirect band gap Γ - X curves occurs at 5.69, 13.14 and 4.24 GPa in LiCdP, LiCdAs and LiCdSb, respectively. The variation of the direct (Γ - Γ) and indirect (Γ - X) band gaps for LiCdN, LiCdP, LiCdAs and LiCdSb are fitted to the following quadratic functions:

$$E_g^{(\Gamma-\Gamma)}(\text{LiCdN}) = 0.32 + 2.25 \times 10^{-2}p - 3.23 \times 10^{-4}p^2$$

$$E_g^{(\Gamma-X)}(\text{LiCdN}) = 3.10 + 0.80 \times 10^{-2}p - 1.43 \times 10^{-4}p^2$$

$$E_g^{(\Gamma-\Gamma)}(\text{LiCdP}) = 1.65 + 5.45 \times 10^{-2}p - 9.085 \times 10^{-4}p^2$$

$$E_g^{(\Gamma-X)}(\text{LiCdP}) = 2.06 - 2.28 \times 10^{-2}p + 2.40 \times 10^{-4}p^2$$

$$E_g^{(\Gamma-\Gamma)}(\text{LiCdAs}) = 0.956 + 5.63 \times 10^{-2}p - 9.51 \times 10^{-4}p^2$$

$$E_g^{(\Gamma-X)}(\text{LiCdAs}) = 1.82 - 2.41 \times 10^{-2}p + 2.97 \times 10^{-4}p^2$$

$$E_g^{(\Gamma-\Gamma)}(\text{LiCdSb}) = 1.098 + 7.71 \times 10^{-2}p - 14.10 \times 10^{-4}p^2$$

$$E_g^{(\Gamma-X)}(\text{LiCdSb}) = 1.548 - 2.44 \times 10^{-2}p + 4.468 \times 10^{-4}p^2$$

The energy is in eV and the pressure p is in GPa.

The effective charge-carrier mass is one of the main factors that determine the transport properties and electrical conductivity of a material. In general, smaller effective masses of the carriers correspond to the faster photogenerated carriers. Consequently, a low effective mass can promote carrier migration and suppress carrier recombination. Here, the effective charge-carrier mass m^* was evaluated by fitting the E - k diagram near the valence-band maximum (VBMA) and the conduction-band minimum (CBMi) with a parabolic variation. The effective mass m^* (in unit of m_0 , where m_0 denotes the electron rest mass) at a given point along the direction given by \vec{k}^{\rightarrow} is:

$$\frac{1}{m^*} = \frac{m_0 \partial^2 E(k)}{\hbar^2 \partial^2 k}$$

The evaluated effective charge-carrier masses, at the Γ point from the band dispersions of the VBMA and CBMi towards the X and L directions in the Brillouin zone, are summarized in Table 3 for the four considered materials. The effective electron mass, the heavy-hole mass and the light-hole mass are indicated by the subscripts “e” (m_e^*), “hh” (m_{hh}^*), and “hl” (m_{hl}^*), respectively. The calculated CB electron effective mass of LiCdN is slightly lower than those of LiCdP, LiCdAs and LiCdSb. Consequently, the mobility of the CB electrons and the electrical conductivity in LiCdN should be slightly higher. From Fig. 2, we note that (i) the electronic states at the conduction-band minimum are more dispersive than the topmost valence-band states; consequently, the conduction-band electrons have lower effective masses than the valence-band heavy holes, and the influence of the latter on the electrical conductivity is minimal; (ii) the effective masses of electrons in the considered materials for the $\Gamma \rightarrow X$ and $\Gamma \rightarrow L$ directions in the BZ are practically equal; hence, the conduction-band electron mobility

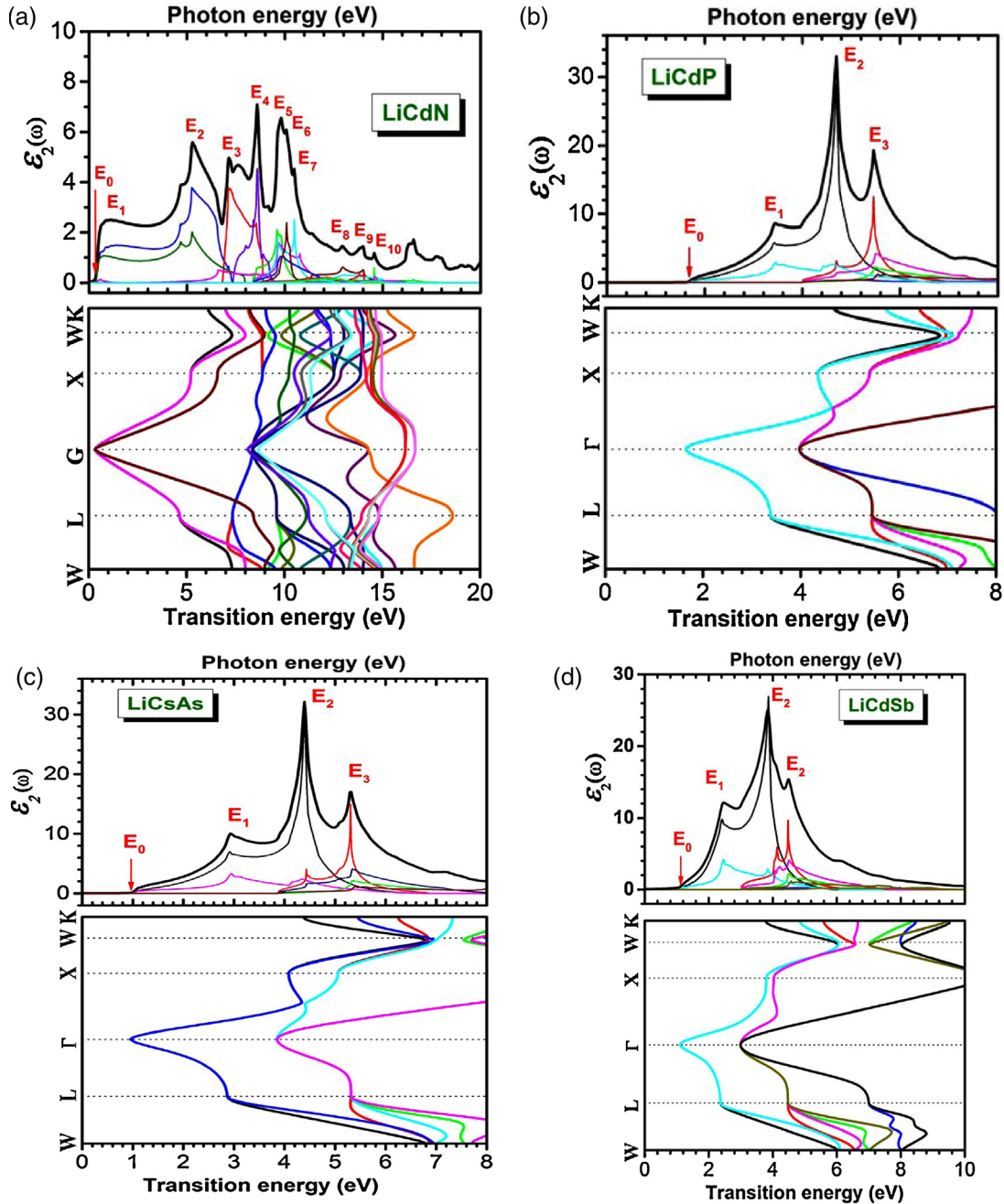


Fig. 6. (a) The decomposition of the imaginary part of the dielectric function into band-to-band contribution (upper panel) and the transition energy band structure (lower panel) for LiCdN. The counting of the bands is down (up) from the top (bottom) of the valence (conduction) band. (b) The decomposition of the imaginary part of the dielectric function into band-to-band contribution (upper panel) and the transition energy band structure (lower panel) for LiCdP. The counting of the bands is down (up) from the top (bottom) of the valence (conduction) band. (c) The decomposition of the imaginary part of the dielectric function into band-to-band contribution (upper panel) and the transition energy band structure (lower panel) for LiCdAs. The counting of the bands is down (up) from the top (bottom) of the valence (conduction) band. (d) The decomposition of the imaginary part of the dielectric function into band-to-band contribution (upper panel) and the transition energy band structure (lower panel) for LiCdSb. The counting of the bands is down (up) from the top (bottom) of the valence (conduction) band.

and the electrical conductivity of the studied materials should be isotropic; (iii) the heavy holes have higher effective masses than the light holes, which indicates the anisotropy between heavy- and light-hole masses; and (iv) the dependence of the effective masses of the heavy holes on the crystallographic direction demonstrates the anisotropy of this property; hence, the valence-band heavy hole conductivity should also be anisotropic.

To understand the nature of the band structures in the investigated compounds, orbital-resolved partial densities of

states (PDOSs) spectra calculated using TB-mBJ functional are presented in Fig. 4. The calculated DOS spectra show similarities for the four investigated materials. The first group of valence bands, if we start from lower energies, reflects the group V atom (i.e., N, P, As and Sb) *s* states. The second one consists of the Cd *d* states with small contributions from the column V atom *s* and *p* states; the contribution of the *s* states increases in this sequence, LiCdN → LiCdP → LiCdAs → LiCdSb, whereas the contribution of the *p* states decreases following that sequence. The rest of the valence

Table 4

Calculated static dielectric constant $\epsilon_1(0)$ and static refractive index of the LiCdN, LiCdP, LiCdAs and LiCdSb compounds compared with the available literature.

	LiCdN	LiCdP	LiCdAs	LiCdSb
$\epsilon_1(0)$	7.52	7.88	9.32	10.93
	6.898 [38]	7.568 [38] 12.205 [34]	8.09 [38] 15.46 [35]	
$n(0)$	2.742	2.808	3.053	3.307
	2.626 [38]	2.751 [38] 3.4936 [34]	2.844 [38] 3.932 [35]	

and conduction bands are mixture of *s* and *p* states of the constituent elements with small contributions from the *d* states atoms.

3.3. Optical properties

The calculated imaginary parts $\epsilon_2(\omega)$ of the frequency-dependent dielectric function for the four considered materials based on the band results discussed in the preceding section are shown in Fig. 5. The behavior of $\epsilon_2(\omega)$ is rather similar for the LiCdP, LiCdAs and LiCdSb compounds with some differences in details.

Table 5

Peak positions of the $\epsilon_2(\omega)$ spectrum together with the dominant interband transition contributions to every peak and their location in the Brillouin zone of LiCdN.

Optical structures		Dominant interband transition contributions		
Structure	Peak position	Transition	Region	Energy (eV)
E_0	0.32	(V_1-C_1)	$\Gamma-\Gamma$	0.32
E_1	0.90	(V_1-C_1)	L- Γ -X	1.33
		(V_2-C_1)	L- Γ -X	0.80
		(V_3-C_1)	L- Γ -X	0.6
E_2	5.32	(V_1-C_1)	W-L, X-W	5.25
		(V_2-C_1)	W-L, Γ -X-W	4.71, 5.26
E_3	7.17	(V_1-C_2)	W-L	7.14
		(V_3-C_1)	L- Γ , X-W	6.64
E_4	8.60	(V_1-C_2)	W-L, Γ -X, W-K	8.49
		(V_2-C_2)	W-L, Γ -X	8.64
		(V_3-C_1)	W-L, X-W-K	8.43
E_4	9.81	(V_1-C_3)	W-L- Γ -X	9.58
		(V_1-C_4)	W-L, Γ -X	9.64
		(V_2-C_3)	L- Γ -X	9.58
		(V_2-C_4)	W-L, Γ -X	9.89
E_5	10.08	(V_2-C_4)	W-L, Γ -X	9.89
		(V_3-C_2)	W-L- Γ -X	10.12
E_6	10.50	(V_1-C_4)	W-L, Γ -X	10.73
		(V_2-C_3)	W-L, Γ -X-W-K	10.44
E_7	12.93	(V_1-C_5)	Γ -X-W	12.95
		(V_2-C_5)	Γ -X-W	13.07
		(V_3-C_3)	W-L- Γ -X-W-K	11.92
		(V_4-C_1)	W-L, X-W-K	12.34
		(V_7-C_1)	W-L, X-W	12.13
		(V_8-C_1)	W-L, X-W	12.13
E_8	13.93	(V_1-C_5)	L- Γ -X-W-K	14.03
		(V_3-C_4)	W-L, W-K	14.03
		(V_3-C_5)	Γ -X	13.61
		(V_4-C_2)	W-L	13.17
E_9	14.58	(V_5-C_2)	W-L- Γ , W-K	14.34
		(V_6-C_2)	W-L- Γ -X-W-K	14.55
		(V_7-C_2)	W-L, Γ -X-W-K	14.55
		(V_8-C_2)	W-L, W-K	14.6

Table 6

Peak positions of the $\epsilon_2(\omega)$ spectrum together with the dominant interband transition contributions to every peak and their location in the Brillouin zone of LiCdP.

Optical structures		Dominant interband transition contributions		
Structure	Peak position	Transition	Region	Energy (eV)
E_0	1.65	(V_1-C_1)	$\Gamma-\Gamma$	1.65
E_1	3.447	(V_1-C_1)	W-L, Γ -X	3.44
		(V_2-C_1)	W-L, Γ -X	3.44
E_2	4.688	(V_1-C_1)	W-L, X-W-K	4.69
		(V_1-C_2)	L- Γ -X	4.69
		(V_2-C_1)	W-L, X-W	4.66
E_3	5.46	(V_1-C_2)	L- Γ -X	5.40
		(V_1-C_3)	W-L, Γ -X	5.51
		(V_1-C_4)	L- Γ -X	5.23
		(V_2-C_2)	W-L, X-W	5.51
		(V_2-C_3)	W-L, Γ -X	5.59

Table 7

Peak positions of the $\epsilon_2(\omega)$ spectrum together with the dominant interband transition contributions to every peak and their location in the Brillouin zone of LiCdAs.

Optical structures		Dominant interband transition contributions		
Structure	Peak position	Transition	Region	Energy (eV)
E_0	0.96	(V_1-C_1)	$\Gamma-\Gamma$	0.96
E_1	2.930	(V_1-C_1)	W-L, Γ -X	2.94
		(V_2-C_1)	W-L, Γ -X	2.97
E_2	4.390	(V_1-C_1)	W-L, Γ -X-W	4.42
		(V_1-C_2)	L- Γ -X	4.46
		(V_2-C_1)	W-L, Γ -X-W	4.34
E_2	4.390	(V_2-C_2)	W-L, X-W	4.50
E_3	5.30	(V_1-C_2)	W-L- Γ , X-W	5.30
		(V_1-C_3)	W-L, Γ -X	5.36
		(V_2-C_2)	W-L- Γ , X-W	5.11, 5.32

The $\epsilon_2(\omega)$ spectrum of the LiCdN compound is quite different from the three others; it is too broad and contains more structures than those of LiCdP, LiCdAs and LiCdSb.

It is worthwhile to attempt to identify the microscopic origin of the transitions that are responsible for the peaks and features in $\epsilon_2(\omega)$. The imaginary part of the dielectric function is determined by the allowed direct electronic transitions between each pair of occupied and unoccupied bands. Therefore, the origins of different

Table 8

Peak positions of the $\epsilon_2(\omega)$ spectrum together with the dominant interband transition contributions to every peak and their location in the Brillouin zone of LiCdSb.

Optical structures		Dominant interband transition contributions		
Structure	Peak position	Transition	Region	Energy (eV)
E_0	1.10	(V_1-C_1)	$\Gamma-\Gamma$	1.10
E_1	2.46	(V_1-C_1)	W-L, Γ -X	2.459
		(V_2-C_1)	W-L, Γ -X	2.46
E_2	3.84	(V_1-C_1)	W-L, X-W-K	3.88
		(V_1-C_4)	L- Γ -X	3.54
		(V_2-C_1)	W-L, X-W	3.88
E_3	4.48	(V_1-C_2)	W-L- Γ -X-W	4.10, 4.56
		(V_1-C_3)	W-L, Γ -X	4.52
		(V_1-C_4)	L- Γ -X	4.75
		(V_2-C_2)	W-L- Γ , X-W	4.23, 4.50
		(V_2-C_3)	W-L, Γ -X	4.527

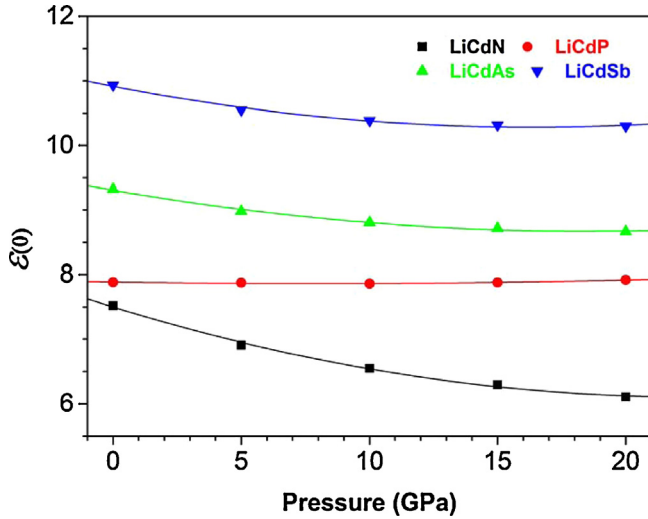


Fig. 7. Variation of the static dielectric function $\epsilon(0)$ as a function of pressure for the LiCdN, LiCdP, LiCdAs and LiCdSb compounds.

structures of the optical spectra can be determined by decomposing each spectrum into its individual pair contribution, i.e., the contribution from each direct electronic transition from the occupied valence state V_i to the empty conduction state $C_j(V_i \rightarrow C_j)$. This technique informs us about the bands that contribute more to the peaks of the $\epsilon_2(\omega)$ spectrum. In order to determine the locations in the BZ of the electronic states that are involved in these transitions, the electronic transition energy $E_{ij}(k) = E_{C_j}(k) - E_{V_i}(k)$ are plotted along the high-symmetry directions in the BZ. In Fig. 6 a, b, c and d, the top panel shows the dominant contributions to

$\epsilon_2(\omega)$ from the interband transitions, and the bottom panel shows the locations of these transitions in the BZ for the four considered materials. The first critical point E_0 of $\epsilon_2(\omega)$ is the edge of the optical absorption. This point is the $\Gamma_V - \Gamma_C$ splitting, which gives the threshold of the direct optical transition between the topmost valence band V_1 and the bottommost conduction band $C_1(V_1 \rightarrow C_1)$ (transition); the counting of the bands is down (up) from the top (bottom) of the valence (conduction) band. This edge is known as the fundamental absorption edge. This first critical point is followed by a number of structures E_i . The locations of the major peaks E_i with the dominant contributions from the interband transitions to each peak and their locations in the Brillouin zone for all four compounds are reported in Tables 5–8.

The results for the dispersive part of the dielectric function, $\epsilon_1(\omega)$ for the four considered materials are given in Fig. 5. The main features in the $\epsilon_1(\omega)$ curves of LiCdP, LiCdAs and LiCdSb are: a peak at around 4 eV; an abrupt decrease to the zero value, after which $\epsilon_1(\omega)$ becomes negative, a minimum at about 6 eV, followed by a slow increase toward zero. The static dielectric constant $\epsilon_1(0)$ is given by the low energy limit of $\epsilon_1(\omega)$. The calculated static dielectric constants $\epsilon_1(0)$ for the studied materials are listed in Table 4 in comparison with the available theoretical results. Our calculated values of $\epsilon_1(0)$ agree rather well with those previously calculated by Mehnane et al. [38] using the full-potential (linear) augmented plane wave plus local orbitals (L/APW+lo) with the standard GGA-PBE [61], but they are somewhat smaller compared to those reported in Ref. [34] using pseudopotential plane wave method. The value of $\epsilon_1(0)$ increases with the increase of the atomic number of the group V elements. In addition, Fig. 7 shows the pressure dependence of $\epsilon_1(0)$. For all the considered compounds, we have got negative values for $d\epsilon_1(0)/dp$, which is nearly 0 for LiCdP.

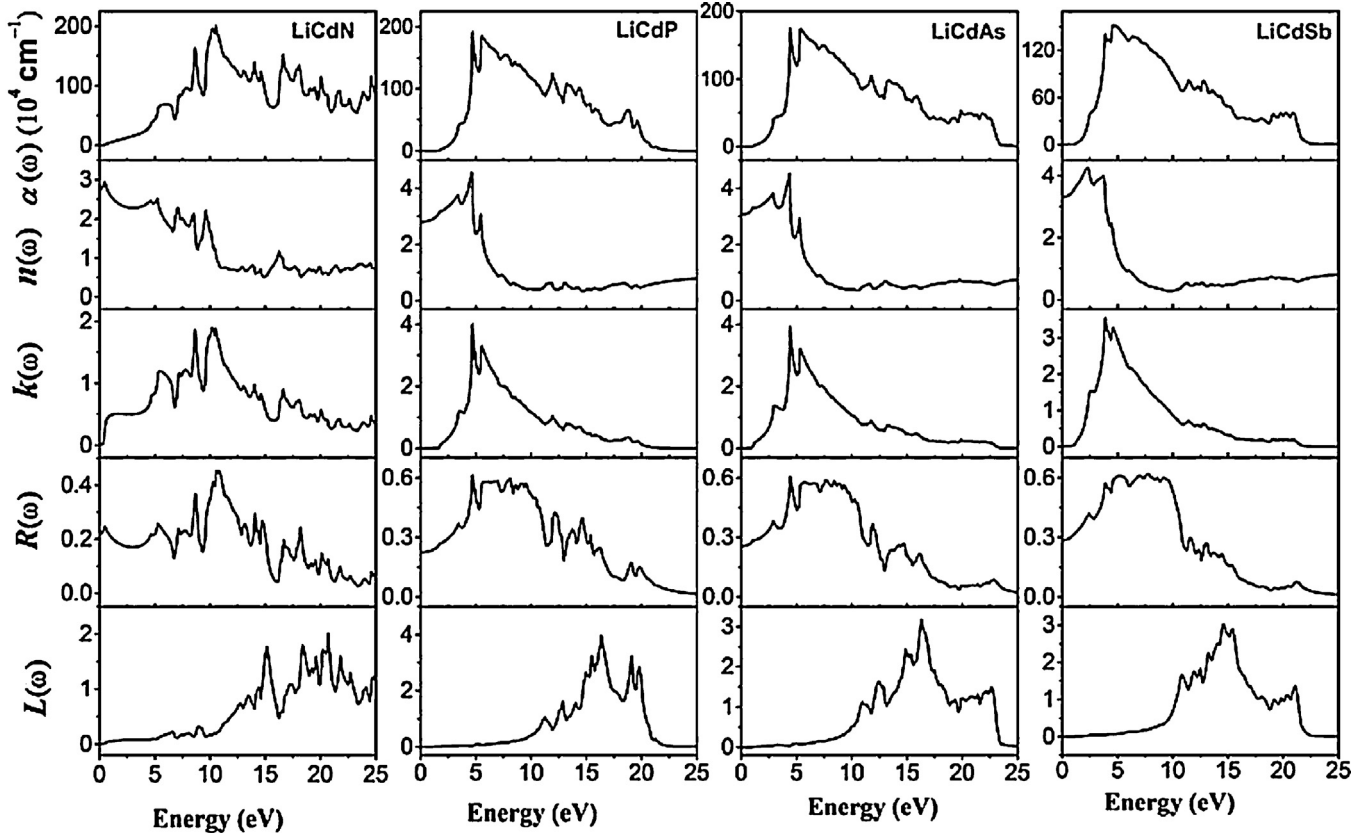


Fig. 8. Calculated absorption coefficient, refractive index, extinction coefficient, reflectivity and energy-loss function spectra of the LiCdN, LiCdP, LiCdAs and LiCdSb compounds as calculated using the TB-mBJ potential.

Fig. 8 presents the absorption coefficient $\alpha(\omega)$, the refractive index $n(\omega)$, extinction coefficient $k(\omega)$, reflectivity $R(\omega)$ and electron energy-loss function $L(\omega)$ spectra of all considered compounds. Fig. 8 shows the close resemblance of the optical spectra between LiCdP, LiCdAs and LiCdSb. The optical spectra of LiCdN are quite different from those of the three other ones. These materials have large absorptions which are suitable for photovoltaic applications. Like the fundamental gap and the static dielectric constants $\epsilon_1(0)$, the static refractive index $n(0)$ is a very important physical quantity for semiconductors. Our obtained values of $n(0)$ for the four considered compounds are listed in Table 4 and compared with the available theoretical results. Our obtained values for $n(0)$ are rather in good agreement with those reported in [38].

4. Conclusion

We have investigated the full range of the electronic and optical properties of the Nowotny–Juza filled-tetrahedral compounds LiCdX (X = N, P, As and Sb) using the full potential augmented plane wave plus local orbitals with four different functionals to the exchange and correlation potential. By using the newly developed functional TB–mBJ, we have obtained better values for the band gaps compared to the standard functionals, with respect to the available experimental results. The four investigated materials are found to be semiconductors possessing a direct band gap located at Γ -point, with gaps ranging from 0.32 to 1.65 eV. Under pressure, the energy band gap of these compounds changes from direct (Γ – Γ) to indirect (Γ –L), except for LiCdN which keeps a direct band gap for the studied pressure range. The calculated optical spectra of the LiCdP, LiCdAs and LiCdSb compounds are quite similar. The optical spectra of LiCdN show more peaks and features than the other considered materials. The microscopic origin of the peaks in the optical spectra and the contributions of the different regions in the Brillouin zone have been identified. These materials have large absorption coefficients which are suitable for photovoltaic applications.

Acknowledgements

The authors (Bouhemadou, Bin-Omran and Khenata) extend their appreciation to the Deanship of Scientific Research at King Saud University for funding the work through research group project No RGP-VPP-088.Y. Al-Douri would like to acknowledge TWAS-Italy for the full support of his visit to JUST-Jordan under a TWAS-UNESCO Associateship. For the author A.H. Reshak, the result was developed within the CENTEM project, reg. no. CZ.1.05/2.1.00/03.0088, co-funded by the ERDF as part of the Ministry of Education, Youth and Sports OP RDI programme.

References

- [1] H. Nowotny, K. Bachmayer, *Monatsh. Chem.* **81** (1950) 488.
- [2] R. Juza, F. Hund, *Z. Anorg. Chem.* **275** (1948) 1.
- [3] D.M. Wood, A. Zunger, R. de Groot, *Phys. Rev. B* **31** (1985) R2570.
- [4] A.E. Carlsson, A. Zunger, D.M. Wood, *Phys. Rev. B* **32** (1985) R1386.
- [5] S.-H. Wei, A. Zunger, *Phys. Rev. Lett.* **56** (1986) 528.
- [6] R. Bacewicz, T.F. Ciszek, *Appl. Phys. Lett.* **52** (1988) 1150.
- [7] R. Bacewicz, T.F. Ciszek, *Mater. Res. Bull.* **23** (1988) 1247.
- [8] K. Kuriyama, F. Nakamura, *Phys. Rev. B* **36** (1987) 4439.
- [9] K. Kuriyama, T. Kato, H. Matsuno, *J. Cryst. Growth* **166** (1996) 631.
- [10] K. Kuriyama, R. Taguchi, K. Kushida, K. Ushiyama, *J. Cryst. Growth* **198/199** (1999) 802.
- [11] K. Kuriyama, K. Kushida, R. Taguchi, *Solid State Commun.* **108** (1998) 429.
- [12] K. Kuriyama, Y. Takahashi, K. Tomizawa, *Phys. Rev. B* **47** (1993) 13861.
- [13] K. Kuriyama, T. Katoh, *Phys. Rev. B* **37** (1988) R7140.
- [14] K. Kuriyama, T. Kato, K. Kawada, *Phys. Rev. B* **49** (1994) 11452.
- [15] K. Kuriyama, T. Kato, T. Tanaka, *Phys. Rev. B* **49** (1994) 4511.
- [16] K. Kuriyama, K. Nagasawa, K. Kushida, *J. Cryst. Growth* **237–239** (2002) 2019.
- [17] K. Kuriyama, K. Kushida, *J. Appl. Phys.* **87** (2000) 2303.
- [18] K. Kuriyama, K. Kushida, *J. Appl. Phys.* **87** (2000) 3168.
- [19] K. Kuriyama, Y. Yamashita, T. Ichikawa, *Phys. Rev. B* **75** (2007) 233204.
- [20] K. Kuriyama, T. Ichikawa, *Phys. Rev. B* **72** (2005) 233201.
- [21] H.C. Kandpal, C. Felser, R. Seshardri, *J. Phys. D: Appl. Phys.* **39** (2006) 776.
- [22] D.M. Wood, W.H. Strohmayer, *Phys. Rev. B* **71** (2005) 193201.
- [23] A. Mellouki, L. Kalarasse, B. Bennecer, F. Kalarasse, *Comput. Mater. Sci.* **42** (2008) 1775.
- [24] A. Mellouki, L. Kalarasse, B. Bennecer, F. Kalarasse, *Comput. Mater. Sci.* **44** (2009) 876.
- [25] F. Kalarasse, B. Bennecer, A. Mellouki, L. Kalarasse, *Comput. Mater. Sci.* **43** (2008) 791.
- [26] F. Kalarasse, B. Bennecer, *J. Phys.: Condens. Matter* **18** (2006) 7237.
- [27] S. Djeroud, L. Kalarasse, B. Bennecer, H. Salmi, F. Kalarasse, *J. Phys. Chem. Solids* **70** (2009) 26.
- [28] A. Mellouki, B. Bennecer, F. Kalarasse, *J. Phys.: Condens. Matter* **21** (2009) 305402.
- [29] F. Kalarasse, B. Bennecer, *J. Phys. Chem. Solids* **67** (2006) 846.
- [30] F. Kalarasse, B. Bennecer, *J. Phys. Chem. Solids* **67** (2006) 1850.
- [31] L. Kalarasse, B. Bennecer, A. Mellouki, F. Kalarasse, *J. Phys. Chem. Solids* **68** (2006) 2286.
- [32] A. Bouhemadou, R. Khenata, F. Zerarga, *Solid State Commun.* **141** (2007) 288.
- [33] A. Bouhemadou, R. Khenata, *J. Phys. Chem. Solids* **68** (2007) 549.
- [34] A. Bouhemadou, R. Khenata, *Semicond. Sci. Technol.* **23** (2008) 105024.
- [35] A. Bouhemadou, *Mat. Sci. Semicond. Process.* **12** (2009) 198.
- [36] A. Bouhemadou, R. Khenata, D. Rached, B. Amrani, *Comput. Mater. Sci.* **49** (2010) 64.
- [37] D. Kieven, R. Klenk, S. Naghavi, C. Felser, T. Gruhn, *Phys. Rev. B* **81** (2010) 075208.
- [38] H. Mehnane, B. Bekkouche, S. Kacimi, A. Hallouche, M. Djermouni, A. Zaoui, *Superlattices Microstruct.* **51** (2012) 772.
- [39] A. Djied, H. Khachai, T. Seddik, R. Khenata, A. Bouhemadou, N. Guechi, G. Murtaza, S. Bin-Omran, Z.A. Alahmed, M. Ameri, *Comput. Mater. Sci.* **84** (2014) 396.
- [40] A. El Maslout, J.P. Motte, C. Gleitzer, *J. Solid State Chem.* **7** (1973) 250.
- [41] W.G. Aulbur, L. Jönsson, J.W. Wilkins, *Solid State Phys.* **54** (2000) 1.
- [42] S. Zh. Karazhanov, P. Ravindran, H. Fjellvåg, B.G. Svensson, *J. Appl. Phys.* **106** (2009) 123701.
- [43] C.S. Wang, W.E. Pickett, *Phys. Rev. Lett.* **15** (1983) 597.
- [44] F. Tran, P. Blaha, *Phys. Rev. Lett.* **102** (2009) 226401.
- [45] P. Blaha, K. Schwarz, G.K.H. Madsen, D. Kvasnicka, J. Luitz, *WIEN2k: An Augmented Plane wave+Local Orbitals Program for Calculating Crystal Properties*, University Karlheinz Schwarz Techn. Universität Wien, Wien, Austria, 2013 ISBN 3-031-9501-1-2.
- [46] A.D. Becke, E.R. Johnson, *J. Chem. Phys.* **124** (2006) 221101.
- [47] D. Koller, F. Tran, P. Blaha, *Phys. Rev. B* **83** (2011) 195134.
- [48] Y.S. Kim, M. Marsman, G. Kresse, F. Tran, P. Blaha, *Phys. Rev. B* **82** (2010) 205212.
- [49] D. Koller, F. Tran, P. Blaha, *Phys. Rev. B* **85** (2012) 155109.
- [50] F. Tran, P. Blaha, K. Schwarz, *J. Phys.: Condens. Matter* **19** (2007) 196208.
- [51] J.P. Perdew, Y. Wang, *Phys. Rev. B* **45** (1992) 13244.
- [52] J.P. Perdew, A. Ruzsinszky, G.I. Csonka, O.A. Vydrov, G.E. Scuseria, L.A. Constantin, X. Zhou, K. Burke, *Phys. Rev. Lett.* **100** (2008) 136406.
- [53] E. Engel, S.H. Vosko, *Phys. Rev. B* **47** (1993) 13164.
- [54] H.J. Monkhorst, J.D. Pack, *Phys. Rev. B* **13** (1976) 5188.
- [55] G.B. Bachelet, N.E. Christensen, *Phys. Rev. B* **31** (1985) 879.
- [56] F.D. Murnaghan, *Proc. Natl. Acad. Sci.* **30** (1944) 244.
- [57] F. Birch, *Phys. Rev.* **71** (1947) 809.
- [58] T. Gruhn, *Phys. Rev. B* **82** (2010) 125210.
- [59] J.A. Camargo-Martínez, R. Baquero, *Phys. Rev. B* **86** (2012) 195106.
- [60] P. Dufek, P. Blaha, K. Schwarz, *Phys. Rev. B* **50** (1994) 7279.
- [61] J.P. Perdew, K. Burke, M. Ernzerhof, *Phys. Rev. Lett.* **77** (1996) 3865.